Marine Geology 315–318 (2012) 98–107

Contents lists available at SciVerse ScienceDirect

Marine Geology

journal homepage: www.elsevier.com/locate/margeo

Petrophysical and consolidation behavior of mass transport deposits from the northern Gulf of Mexico, IODP Expedition 308

Brandon Dugan *

Department of Earth Science, Rice University, Houston, TX 77005 USA

ARTICLE INFO

Article history:
Received 30 May 2011
Received in revised form 21 April 2012
Accepted 2 May 2012
Available online 10 May 2012

Communicated by Dr. D.J.W. Piper

Keywords:
petrophysics
consolidation
mass transport deposit
IODP
Gulf of Mexico

ABSTRACT

Mass transport deposits (MTDs) in the Ursa region of the northern Gulf of Mexico have low internal reflectivity, high resistivity, high bulk density, and low porosity in comparison to the hemipelagic sediments that bound them. I infer these MTD properties result from enhanced consolidation related to shear deformation. The deviation of physical properties within MTDs, compared to the bounding mud-rich sediments, increases from west to east in the Ursa region. The largest amount of shear-induced densification occurs at the bases of the MTDs resulting in high amplitude basal reflections, and to a lesser extent high amplitude top reflections, in seismic data. While the deformation paths of MTDs (burial and shear) and bounding hemipelagic sediments (burial) differ, comparison of bulk physical properties indicate that all sediments within the Ursa region have similar bulk density-resistivity and void ratio-effective stress behavior. From density and resistivity data and consolidation experiments, I conclude that shear deformation in MTDs in the Ursa region produces denser, more resistive sediments with porosity decreases up to 6 porosity units. This shearing, however, does not change fabric or general deformation behavior at the bed scale (0.1–1 m). The similar resistivity-void ratio-effective stress trends provide a means to infer some of the bulk physical properties (e.g., permeability) of MTDs from information on normally consolidated mud and from the seismic response.

1. Introduction

Mass transport deposits (MTDs) are sedimentary bodies that have experienced downslope migration and various degrees of internal deformation. MTDs can be the result of submarine slumps, submarine landslides, debris flows, turbidity currents, or other gravity-driven mass movements. The initial sediment properties and mobilization process dictate whether an MTD fails and moves rapidly with long run-out distances (e.g., deposition by turbidity currents), or fails slowly with short run-out (e.g., downslope creep). Hampton et al. (1996) review the environments where submarine landslides occur and the mechanisms that control their initiation. Numerous geophysical studies have documented the distribution and occurrence of MTDs worldwide. McAdoo et al. (2000) used multibeam bathymetry and sidescan sonar surveys to characterize the surface expression and geometry of submarine landslides for distinct tectonic environments along the continental shelf of the United States. Other studies used multi-channel seismic data to look at the subsurface distribution, seismic character, and mechanism of failure of MTDs (e.g., Posamentier, 2004; Sawyer et al., 2007; Bull et al., 2009). Numerical models and stability analyses have been used to describe the evolution of pore fluid pressures and the role of earthquakes in generating slope failures and MTDs (e.g., Kvalstad et al., 2005; Locat et al., 2009; Stigall and Dugan, 2010). I expand MTD research beyond mechanism and distribution by characterizing bulk physical properties of MTDs and their relationship to bounding sediments.

In this study, I assess seismic and petrophysical characters of MTDs and describe how MTDs have porosity–resistivity relationships similar to bounding, non-MTD sediments. This similar behavior can be used to estimate bulk physical properties and the amount of shear deformation of the sediment within the MTDs. I integrate multi-channel seismic (MCS) data and logging-while-drilling (LWD) data to characterize the bulk physical properties of MTDs in the Ursa region of the northern Gulf of Mexico. Resistivity and bulk density data show that MTDs are more consolidated than the uniaxially deformed hemipelagic sediments that bound them. The degree of densification is highest at the base of MTDs, which creates a large impedance contrast. This contrast is recorded in MCS data as a strong, positive reflection at the base of MTDs in the Ursa region. Consolidation experiment data are used to interpret the apparent preconsolidation stress for samples from MTDs and from bounding mud. These results show that MTDs are on the same void ratio-vertical effective stress path as the uniaxially deformed sediment. The integration of seismic, petrophysical, and consolidation data suggests that for shear strains observed in the Ursa region, preferential, bed-scale fabrics are not developed within MTDs.

2. Study region

The Ursa Basin is located in water depths ranging from 1000 to 1300 m on the continental slope 210 km southeast of New Orleans, LA, USA (Fig. 1). This region has been studied extensively because of

* Tel.: +1 713 348 5088.
E-mail address: dugan@rice.edu.

0025-3227/$ – see front matter © 2012 Elsevier B.V. All rights reserved.
doi:10.1016/j.margeo.2012.05.001

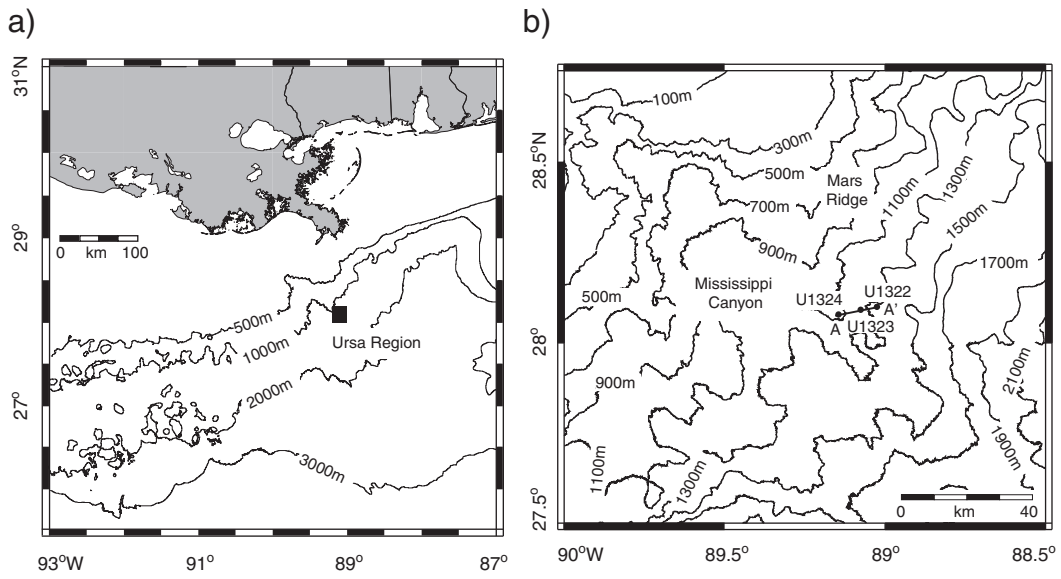

Fig. 1. (a) Regional bathymetric map showing the location of the Ursa region in the Gulf of Mexico, offshore USA. (b) Location of IODP Expedition 308 Sites U1322, U1323, and U1324 on the eastern side of Mississippi Canyon in the Ursa region. All contours are water depth (m).

hydrocarbon reservoirs at depth, and because of drilling problems associated with flow of unconsolidated sands from the shallow subsurface to the seafloor (Pelletier et al., 1999; Ostermeier et al., 2000). These studies have benefited from the existence of high resolution seismic data (exploration and hazard) and industry and geotechnical wells. Integrated Ocean Drilling Program (IODP) Expedition 308 completed a shallow (<650 mbsf) coring and logging program in the Ursa region to address the coupling between sedimentation, overpressure, fluid flow, and slope stability in shallow sediments along passive margins (Flemings et al., 2006; Dugan and Germaine, 2008; Flemings et al., 2008).

Extensive seismic data coverage of the Mississippi Canyon region, within which the Ursa basin is located, allow interpretation of regional depositional systems. The general study region is characterized by four channel–levee systems that are oldest in the east (Ursa) and youngest in the west (Young Timbalier) (Sawyer et al., 2007). All of the sediments within these channel–levee systems are younger than ~60 kyr, and were sourced by the Mississippi River (Winker and Booth, 2000; Sawyer et al., 2007). The generalized evolution of the systems includes an evacuated channel with channel-margin slides, filling of the channel with coarse-grained material (e.g., sand), and finer-grained (e.g., silt and clay) levee deposits flanking the channels. Lithologic control across the region is defined by seismic character and correlation with gamma ray log data. Due to the westward migration of the system, the eastern channels and their levee deposits are buried by the fine-grained levee deposits of the younger channel–levee systems. Mass transport deposits that extend across the region have been identified in the fine-grained levee deposits. Based on the fact that all the MTDs are younger than 60 kyr, are localized in levee deposits, are sourced from Mississippi River, and have similar gamma ray signatures, it is interpreted that the regional MTDs are composed of silt and clay.

Sawyer et al. (2007) interpreted the headscarps of some of the regional MTDs allowing documentation of the original failure region within the levee deposits. Basin-scale fluid flow and stability modeling (Stigall and Dugan, 2010) and failure evolution modeling (Sawyer et al., 2009) show that these MTDs originated as hemipelagic levee deposits, similar to the regional trend, but fluid overpressures helped promote failure as discrete events. Building on the regional seismic characterization and modeling studies, I interpret that the sediments within the MTDs were initially normally consolidated levee deposits that failed.

IODP cores and high resolution seismic data provide a more detailed image of the Ursa region and its sediments. The late Pleistocene depositional history of the shallow sedimentary section in the Ursa region includes a regional, sand-dominated aquifer (the Blue Unit) that is overlain by mud-dominated sediments (Winker and Booth, 2000; Sawyer et al., 2007). The Blue Unit is composed of sands interbedded with mud. Some of the sands are continuous across this basin whereas others have been truncated by the incision of channel complexes (Sawyer et al., 2007) (Fig. 2). The sediments deposited on the Blue Unit were primarily sourced by submarine channel–levee systems over the last 60 kyr as described by Sawyer et al. (2007). These supra-Blue Unit sediments contain numerous MTDs of variable thickness and extent. MTD1 (Fig. 2) has been interpreted as a series of stacked, discrete failures with seismically identifiable headscarps; MTD2 (Fig. 2) does not have an identifiable headscarp region as the MTD extends outside the 3D seismic data sets available for interpretation (Sawyer et al., 2007). The sediments overlying the Blue Unit are 620 m thick near Site U1324 and thin to 240 m at Site U1322 (Fig. 2). The uppermost, near-seafloor section (0–50 mbsf) is composed of hemipelagic mud that is continuous across the region. Based on biostratigraphic analysis of the near-seafloor section, sediments shallower than 50 mbsf have been deposited in the last 18 kyr (Flemings et al., 2006). A subtle sediment fining exists from west to east with Site U1324 being dominated by clayey silt and Site U1322 being primarily silty clay (Sawyer et al., 2008). In situ measurements and consolidation experiments on geotechnical cores document shallow overpressure in the Ursa region (Eaton, 1999; Pelletier et al., 1999; Ostermeier et al., 2000, 2001; Flemings et al., 2006; Dugan and Germaine, 2008; Flemings et al., 2008). The shallow overpressure has been implicated as the driving force for shallow water flows and also as a driving force for slope failure (Sawyer et al., 2009; Stigall and Dugan, 2010).

3. Data and methods

3.1. Multi-channel seismic data

High-quality multi-channel seismic (MCS) data have been collected over the Ursa region by industry for geohazard analysis. Geohazard surveys in the region provide very high resolution seismic imaging of the sediments bounding the Blue Unit. Sawyer et al. (2007) used these data to evaluate the regional depositional systems in the Ursa

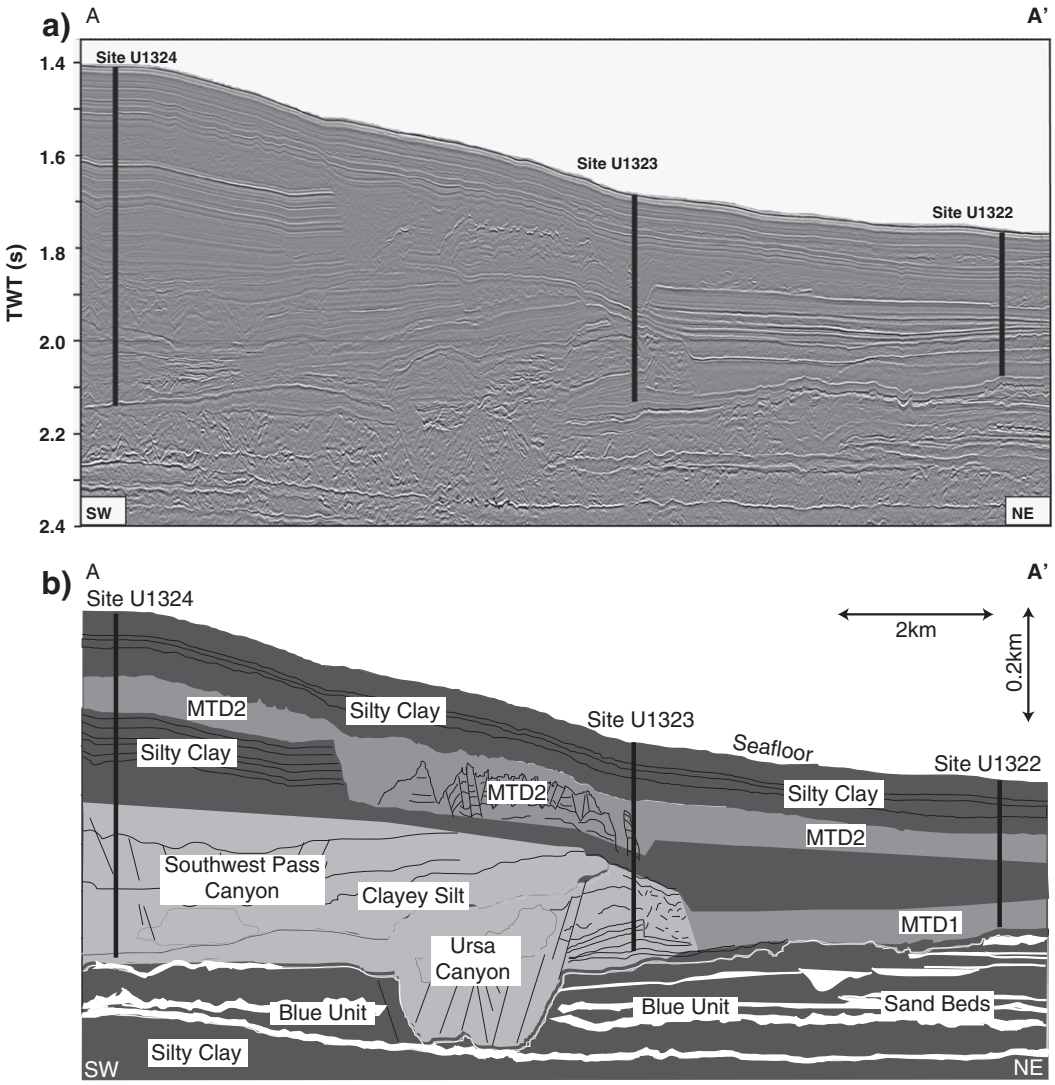

Fig. 2. (a) High resolution, multi-channel seismic cross-section A–A′ (located in Fig. 1b) through IODP Sites U1324, U1323, and U1322. (b) Line drawing of interpreted seismic cross-section A–A′. MTD indicates regions that have been interpreted as mass transport deposits based on seismic data, petrophysical data, and core analyses (Flemings et al., 2006; Sawyer et al., 2009). Silty clay, sand beds, and clayey silt are interpreted lithology from core and logging analyses.

region and to define the general evolution of the submarine canyon and levee systems. I focus on the upper 650 mbsf along the Ursa transect studied by IODP Expedition 308 where the MCS data have a vertical resolution of 3–5 m and a horizontal resolution of 6.25 m.

3.2. Log data

Logging-while-drilling (LWD) data collected during IODP Expedition 308 at Sites U1324, U1323, and U1322 (Flemings et al., 2006) are used to evaluate the petrophysical properties of sediments in the Ursa region. I focus on the gamma ray, resistivity, and bulk density logs. The gamma ray data provide a lithologic guide where higher values reflect higher clay content. The resistivity log provides information on the proportion of solid grains and pore fluids and resistivity of the components (Archie, 1942). For the MTD analysis, I use the phase-shift resistivity data to evaluate deformation however, other resistivity log data collected during IODP Expedition 308 yield similar results. The bulk density log constrains porosity at the sites, which I also use to define deformation. Porosity $[\phi = (\rho_b - \rho_g)/(\rho_w - \rho_g)]$ is calculated from the log-measured bulk density (ρ_b), pore fluid density (ρ_w), and solid grain density (ρ_g). I assume standard seawater density (1.024 g/cm^3) and constant grain density (2.7 g/cm^3) based on observed porewater chemistry and measured grain density (Flemings et al., 2006). LWD-determined porosity is in excellent agreement with the core-measured porosity in the clay-dominated sections (Flemings et al., 2006). I use the LWD data because it provides better resolution than the core measurements.

LWD operations were completed with a target penetration rate of 30 m/h; the exception to this was Site U1322 where drilling proceeded at 20 m/h below ~195 mbsf (Flemings et al., 2006). All log data were recorded in time and re-sampled at 0.1 m for analysis. Time data are converted to depth using the Schlumberger Integrated Drilling and Logging system, which records time and depth of the drill string below the rig floor and time of each sensor measurement. This is then coupled with the known distance from each sensor to the end of the drill string. This conversion requires high-quality depth data and includes corrections for motion in the derrick, heave of the vessel, and movement of the motion compensator (Flemings et al., 2006). Drilling fluid circulation was limited in the shallow section to minimize borehole and formation disturbance near the sea floor, however some borehole expansion was observed. LWD operations were completed with seawater as the drilling fluid at Site U1322, seawater (above 198 mbsf) and heavy mud (below 198 mbsf) at Site U1323, and seawater (above 472 mbsf) and heavy mud (below 472 mbsf) at Site U1324.

Heavy drilling mud was circulated at depth at Sites U1323 and U1324 to help maintain hole integrity and minimize flow from the overpressured Blue Unit into the borehole.

4. Site characterization

4.1. Site U1324

Site U1324 was drilled through 612 m of sediment overlying the Blue Unit (Fig. 2). One MTD is observed in seismic data at Site U1324 (Fig. 2). The MTD extends from 100 to 160 m below seafloor (mbsf) (Fig. 3). The reflection character of the MTD changes from top to bottom. Above the MTD, reflections are continuous and have high amplitude (Fig. 2). Reflection amplitude and continuity decrease with depth through the MTD. The base of the MTD is clearly defined by a high amplitude reflection. This MTD can be traced to the east to Sites U1323 and U1322 (Fig. 2).

Sediments at Site U1324 from 0 to 360 mbsf are interpreted as mud-dominated based on the high gamma ray (GR) values (Fig. 3). From 360 to 612 mbsf, GR decreases and is variable (Fig. 3) which is indicative of varying lithology and/or poor borehole conditions. These variations reflect alternating silt (low GR) and clay (high GR) layers. Grain-size analyses confirm these lithologic interpretations based on gamma ray data from Site U1324 (Fig. 3). Hydrometer analyses document >50% clay-sized particles above 360 mbsf; below 360 mbsf the silt content increases to 50% or more (Fig. 3). Sawyer et al. (2008) provide details of the grain-size analysis procedure and complete grain-size distribution curves for each sample.

LWD resistivity increases from the seafloor to 100 mbsf (Fig. 3). The top of the MTD is subtle and hard to define, but is identified at 110 mbsf based on small deviations in trend of the gamma ray and resistivity logs and a small step increase in resistivity. Resistivity then increases along a different trend to 160 mbsf where an abrupt decrease occurs. This change defines the base of the MTD. Resistivity is near-constant from 160 to 350 mbsf. Below 350 mbsf resistivity varies, notably where GR decreases abruptly and is erratic. The poor or erratic resistivity log responses below 360 mbsf are likely the result of poor borehole conditions associated with silt interlayers. The caliper log confirmed washouts over this zone. Shipboard sedimentology also confirmed increased silt and sand content in the zones with erratic log responses (Flemings et al., 2006). A higher proportion of coarse-grained sediments would be more susceptible to washout.

The bulk density log generally parallels the resistivity log (Fig. 3). Below 30 mbsf, bulk density gradually increases to 1.95 g/cm^3 at 160 mbsf; below this depth bulk density decreases to 1.9 g/cm^3. This change in density occurs at the base of the seismically identified MTD (Fig. 2). Below 235 mbsf, bulk density increases with depth until the silt interlayers are encountered. The density data are problematic below 360 mbsf because of poor borehole conditions. The bulk density tool is a contact tool, thus data are more sensitive to borehole washout than non-contact tools (e.g., resistivity). The logging density data, therefore, are more erratic and less representative of true formation properties in zones with washout.

Porosity decreases rapidly from 80% at the seafloor to 55% near 50 mbsf (Fig. 3). From 50 to 360 mbsf, porosity decreases to 40%. Within the silt interlayers, porosity appears higher than porosity in the surrounding mud-dominated sections, however this is an artifact of low bulk density in washout zones. A thin, high porosity anomaly at 160 mbsf marks the base of the regional MTD and the top of the underlying mud.

4.2. Site U1323

Site U1323 was drilled through a mud-dominated package to 241 mbsf (Fig. 2). Two MTDs are identified on seismic data at the site. A shallow MTD, near 50 mbsf, is a thin unit that lacks coherent layering, but is bounded by continuous reflections (Figs. 2, 4). The second MTD is deeper in the section, is thicker, and extends from 100 to 195 mbsf.

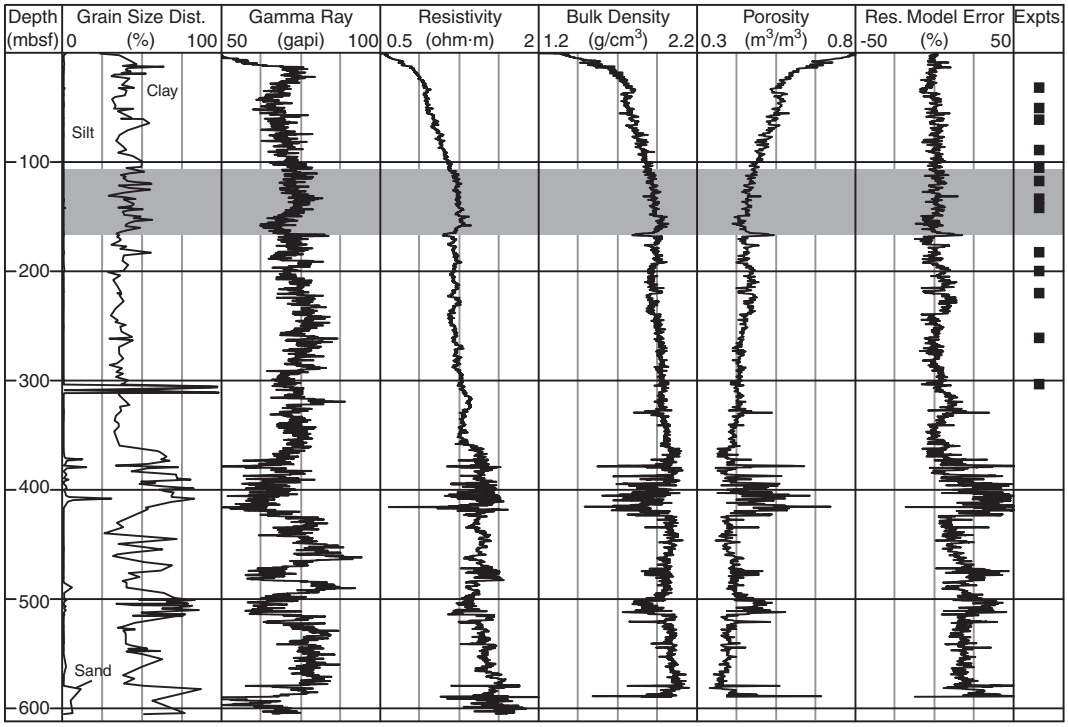

Fig. 3. Grain-size distribution, LWD log data, and resistivity model errors from IODP Site U1324 (located in Fig. 1b). All data are referenced to meters below seafloor (mbsf). Gamma ray, phase-shifted resistivity, and bulk density are LWD data. Porosity is calculated from bulk density assuming constant seawater density (1.024 g/cm^3) and constant grain density (2.7 g/cm^3). Resistivity model error is calculated from Eq. (3). Grey-shaded region is interpreted MTD based on seismic and log character. Expts. identify locations of samples used in consolidation experiments (Long et al., 2008b).

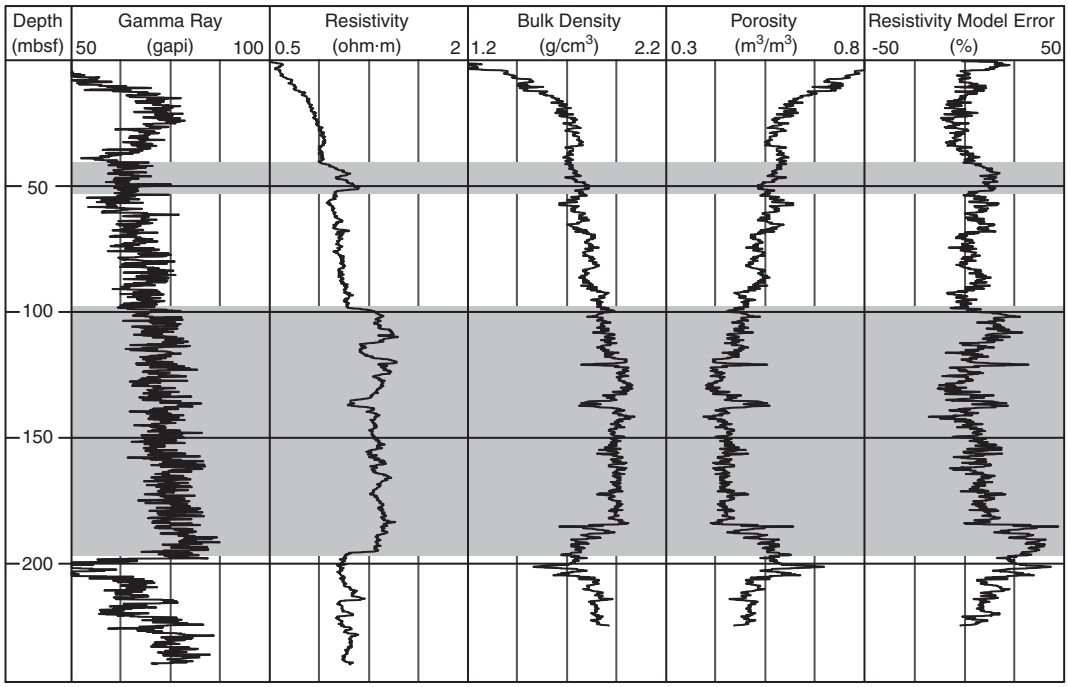

Fig. 4. LWD log data and resistivity model errors from IODP Site U1323 (located in Fig. 1b). All data are referenced to meters below seafloor (mbsf). Gamma ray, phase-shifted resistivity, and bulk density are LWD data. Porosity is calculated from bulk density assuming constant seawater density (1.024 g/cm^3) and constant grain density (2.7 g/cm^3). Resistivity model error is calculated from Eq. (3). Grey-shaded regions are interpreted MTDs based on seismic and log character.

This MTD has low amplitude and chaotic reflections that are bounded by continuous, higher amplitude reflections (Figs. 2, 4). The MTD has a gradational top boundary where reflection amplitude decreases moving from the overlying sediments into the MTD. The base is marked by a regional, high amplitude reflection. This MTD is interpreted as the result of two separate events — one depositing the sediments from 100 to 135 mbsf and a second creating the deposits from 135 to 195 mbsf. The sediments that extend from 100 to 135 can be mapped as an MTD extending to Sites U1322 and U1324 (Fig. 2). Regionally, this MTD is characterized by a sharp basal reflection, a subtle but continuous reflection near its top, and a lack of strong or continuous internal reflections. The basal reflection at Site U1323 is not as pronounced as it is at Sites U1322 and U1324. The deposits from 135 to 195 mbsf lack internal character but have numerous high amplitude reflections that are not continuous. These strong reflections, however, appear to be the result of block rotation within the MTD. This blocky-type failure is locally present near Site U1323 (Fig. 2).

LWD gamma ray increases from the seafloor to 197 mbsf, which reflects clay-dominated sediments (Fig. 4). At 200 mbsf, the gamma ray decreases to less than 50 gapi. This decrease indicates a quartz-rich interval that is presumably fine-grained sand. An increase in annular pressure measured near this horizon is consistent with entering a coarse, permeable horizon that is overpressured (Flemings et al., 2006). This lithologic change ties with the high amplitude reflection that marks the base of the deepest MTD. Gamma ray then increases with depth to the bottom of the hole.

LWD resistivity has two distinct trends at Site U1323 (Fig. 4). Hemipelagic mud has low resistivity with a gradual increase to 100 mbsf. MTDs at Site U1323 are ~10% more resistive than bounding non-MTD, hemipelagic mud and have near-constant resistivity. The shallowest MTD, near 50 mbsf, has a sharp increase in resistivity at its top and its base. The seismically identified MTD package from 100 to 195 mbsf has three distinct high resistivity zones that are bounded by sharp changes to lower resistivity (Fig. 4). Near 135 mbsf, a resistivity decrease separates the two MTDs that exist from 100 to 195 mbsf. Below 200 mbsf, resistivity is lower than in the MTDs and does not vary significantly.

The MTDs at Site U1323 are denser than their bounding mud (Fig. 4). From 0 to 100 mbsf, bulk density increases to 1.9 g/cm^3 consistent with consolidation and burial. This correlates with the gradual increase in resistivity over the same interval. From 100 to 130 mbsf, bulk density increases to ~2.0 g/cm^3. Bulk density then rapidly decreases to 1.75 g/cm^3 by 135 mbsf and then increases to 2.0 g/cm^3 by 145 mbsf. Just below 145 mbsf, bulk density decreases to 1.95 g/cm^3 and is near-constant to 180 mbsf. This density behavior from 100 to 180 mbsf with a slow increase, a local minimum, and then near-constant density zone coincides with three high resistivity zones (Fig. 4). From 180 to 200 mbsf bulk density decreases and reaches another local minimum near the base of the MTDs. Below 200 mbsf, bulk density gradually increases as the clay content increases (Fig. 4).

4.3. Site U1322

Site U1322 is the easternmost site drilled during IODP Expedition 308 and has the thinnest mud section, ~240 m, over the Blue Unit (Figs. 2, 5). Low amplitude reflections in seismic data are used to identify two MTDs at Site U1322 from 35 to 55 and 85 to 125 mbsf (Fig. 5). These low amplitude, non-continuous reflections comprise the interior of the MTDs. The shallow MTD ties seismically with the shallow MTD at Site U1323, and the deeper MTD correlates with MTDs at Sites U1323 and U1324 (Fig. 2). Unlike Sites U1323 and U1324, however, the MTDs at Site U1322 have high amplitude reflections at their tops and bases.

The LWD gamma ray (GR) at Site U1322 increases with depth (Fig. 5), which is characteristic of a mud-dominated section with normal consolidation. Grain-size data confirm that the sediments at Site U1322 are mud-dominated with much of the section composed of >50% clay-sized particles (Fig. 5). Sawyer et al. (2008) provide details of the grain-size analysis procedure and complete grain-size distribution curves for each sample. LWD resistivity, however, is not as uniform. In general, resistivity increases downhole but many different resistivity zones exist. Above 125 mbsf, the resistivity data have two zones with high resistivity (35–57 and 89–123 mbsf). Each of these zones has an abrupt resistivity decrease at its base that corresponds to the high

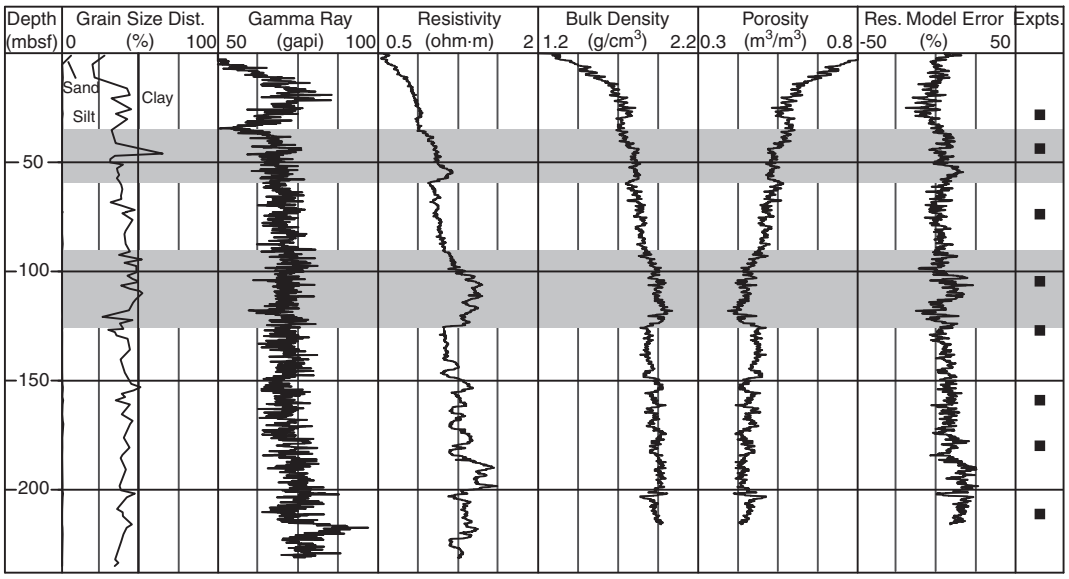

Fig. 5. Grain-size distribution, LWD log data and resistivity model errors from IODP Site U1322 (located in Fig. 1b). All data are referenced to meters below seafloor (mbsf). Gamma ray, phase-shifted resistivity, and bulk density are LWD data. Porosity is calculated from bulk density assuming constant seawater density (1.024 g/cm^3) and constant grain density (2.7 g/cm^3). Resistivity model error is calculated from Eq. (3). Grey-shaded regions are interpreted MTDs based on seismic and log character. Expts. identify locations of samples used in consolidation experiments (Long et al., 2008b).

amplitude reflections at the base of the MTDs. Below 125 mbsf, five, thin low-to-high resistivity cycles exist (Fig. 5). Over this clay-dominated section (Fig. 5), I infer the high resistivity values are indicative of thin, stacked MTDs that were not identified with the MCS data as they are thinner than the seismic resolution. They appear as planar reflections.

LWD bulk density increases in zones of high resistivity and decreases when resistivity decreases (Fig. 5). Bulk density generally increases downhole to 1.96 g/cm^3. The highest bulk density, 2.0 g/cm^3, occurs near 125 mbsf in a high resistivity zone. The density-derived porosity documents sharp changes in porosity between MTDs and their bounding sediments (Fig. 5); these changes at the tops and bases control the seismic character at the tops and bases of the MTDs.

5. Resistivity–porosity model

I use Archie's law (Archie, 1942) to relate resistivity and porosity at these sites. Archie's law states

$$R = aR_w\phi^{-m}S_w{}^{-n}. \quad (1)$$

R is the bulk formation resistivity, R_w is the formation water resistivity, ϕ is the porosity, S_w is the water saturation, and a, m, and n are empirical constants.

The Ursa region is water-saturated ($S_w = 1$) above the Blue Unit so Archie's law simplifies as

$$R = aR_w\phi^{-m}. \quad (2)$$

R_w is calculated assuming pores are filled with seawater and using temperature gradients determined at Sites U1322 and U1324 (Long et al., 2008a). Chemical analyses of the porewaters at Sites U1322 and U1324 confirm that the pores are water-saturated and that the porewaters have near-seawater salinity (Flemings et al., 2006).

I use the shallow, hemipelagic mud from Site U1324 to constrain a and m (Eq. (2)). A regression of measured bulk formation resistivity and porosity from 12.5 to 109 mbsf provides $a = 1.23$ and $m = 1.60$ (Fig. 6). Porosity data were determined from the bulk density LWD data assuming a constant grain density of 2.70 g/cm^3 and an average seawater density of 1.024 g/cm^3. LWD-determined porosity is in excellent agreement with the core-measured porosity in the clay-dominated sections (Flemings et al., 2006). I use the LWD data because it provides the same high resolution sampling of resistivity and porosity.

Using Eq. (2) and the constrained empirical constants, I predict bulk formation resistivity (R_{mod}) from LWD-determined porosity. I present results as resistivity errors (R_{err}) based on the modeled (R_{mod}) and observed (R) resistivity:

$$R_{err} = \frac{R - R_{\mathrm{mod}}}{R} \times 100\%. \quad (3)$$

The resistivity model for Site U1324 successfully predicts resistivity in the mud-dominated section (Fig. 3). From the seafloor to 300 mbsf, model errors are near 0%. The model errors increase to 25–50% below

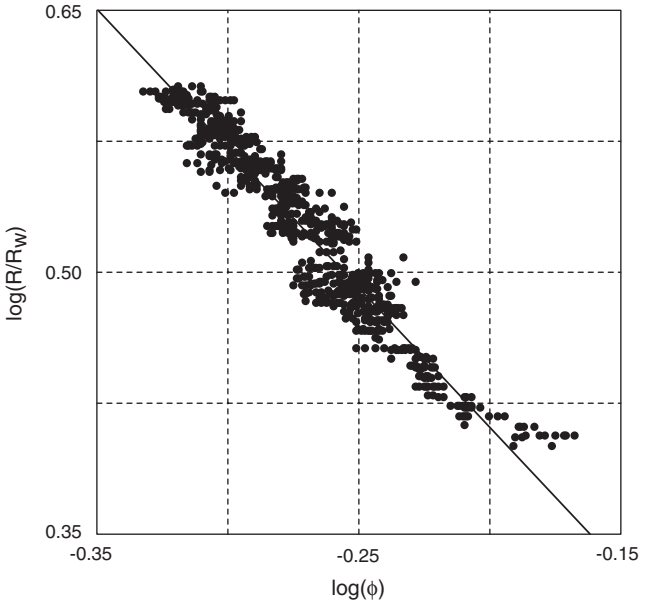

Fig. 6. Regression (solid line) of resistivity and bulk-density-derived porosity data (solid circles) from 12.5 to 109 mbsf at Site U1324. This zone comprises the shallow, non-MTD mud and provides a=1.23 and m=1.60 for Eq. (2).

360 mbsf. This interval, however, has poor quality porosity data due to borehole washout due to an increase in silt content.

At Site U1323, the modeled resistivity is similar to the measured resistivity through most of the section, but there is increased error through the thick MTDs from 100 to 195 mbsf (Fig. 4). Near 100 mbsf, I under-predict the resistivity. This results from a sharp increase in resistivity but a gradual decrease in porosity. At the base of these MTDs, I under-predict the resistivity. This mismatch is caused by near-constant resistivity where porosity is gradually increasing (Fig. 4). This may be the result of poor formation conditions causing degradation in the density measurements as drilling neared the sand-rich horizon at 200 mbsf; resistivity tools are less sensitive to borehole conditions. An enlarged borehole due to sediment washout was observed at the same depth interval as these low bulk density and high porosity values (Flemings et al., 2006), which support the interpretation that borehole conditions yielded degraded log quality from 185 to 205 mbsf.

In general, the model predicts the resistivity behavior at Site U1322 (Fig. 5). I successfully simulate the hemipelagic drape sediments, the two MTDs identified in MCS data, and the stacked MTDs identified with the LWD data. The success with which the model predicts resistivity from porosity within drape sediments, thick MTDs, and thin MTDs across the Ursa basin suggests that MTD mobilization and emplacement has not significantly altered the fabric, and thus porosity-resistivity behavior, in these shallow sediments, even though the physical properties and petrophysical responses are impacted.

6. Consolidation model

Based on the lack of anisotropy of physical properties or development of a fabric in the MTDs, I use uniaxial deformation behavior to estimate the amount of shear-induced porosity loss within MTDs at Sites U1322 and U1324. Uniaxial consolidation during burial is modeled with void ratio-vertical effective stress relationship (Lambe and Whitman, 1969),

$$e = e_o - c_c \log \sigma_v'. \quad (4)$$

e is the void ratio which is related to porosity [$\phi = e/(1+e)$], c_c is the compression index, e_o is the void ratio at 1 kPa vertical effective stress, and σ_v' is the vertical effective stress.

The compression index (c_c) and e_o are determined from laboratory experiments on non-MTD mud (i.e., hemipelagic mud). Long et al. (2008b) provide estimates of in situ vertical effective stress, or preconsolidation stress, and in situ void ratio (Fig. 7) based on constant-rate-of-strain consolidation experiments. Sample locations are indicated in Figs. 3 and 5. In situ stresses are estimated using the work-stress approach (Becker et al., 1987). A regression of the non-MTD void ratio and preconsolidation stress data from Sites U1322 and U1324 provides $e_o = 2.9$ and $c_c = 0.70$ ($R^2 = 0.70$) (Fig. 7).

Based on measured pore pressure, Flemings et al. (2008) constrain that the overpressure, or pressure in excess of hydrostatic, is 60% of hydrostatic vertical effective stress (σ_{vh}') in the mud at Site U1324 and is 70% of σ_{vh}' in the mud at Site U1322. These data provide empirical constraints on in situ effective vertical stress at each site, such that $\sigma_v' = 0.4\sigma_{vh}'$ at Site U1324 and $\sigma_v' = 0.3\sigma_{vh}'$ at Site U1322. With these effective vertical stress estimates and the laboratory-derived e_o (2.9) and c_c (0.70), I model the void ratio for the mudstones in the Ursa region assuming uniaxial strain. For the MTD at Site U1324 (110–160 mbsf), this model predicts an average void ratio of 1.1 ($\phi = 52\%$) due to normal consolidation during burial and does not account for any shear-induced porosity loss. LWD data yield an average void ratio of 1.0 ($\phi = 50\%$) for this interval that has been buried and subject to shear deformation. This analysis indicates that 2 porosity units (52% vs 50%) are lost because of shear consolidation at Site U1324 (Fig. 7). For the same MTD at Site U1322 (85–125 mbsf), the void ratio model predicts an average void ratio of ~1.3 ($\phi = 56\%$) due to burial alone and the average LWD void ratio due to burial and shear is 1.0 ($\phi = 50\%$). This suggests the MTD sediments have lost an average of 6 porosity units (56% vs 50%) due to shear deformation at Site U1322 (Fig. 7). Comparison of shear-induced consolidation between Sites U1322 and U1324 suggests greater shear deformation and porosity loss at Site U1322. This is consistent with grain alignment analyses documenting greater grain alignment and potentially longer run-out distances, or more shear strain, at Site U1322 (Yamamoto et al., 2005).

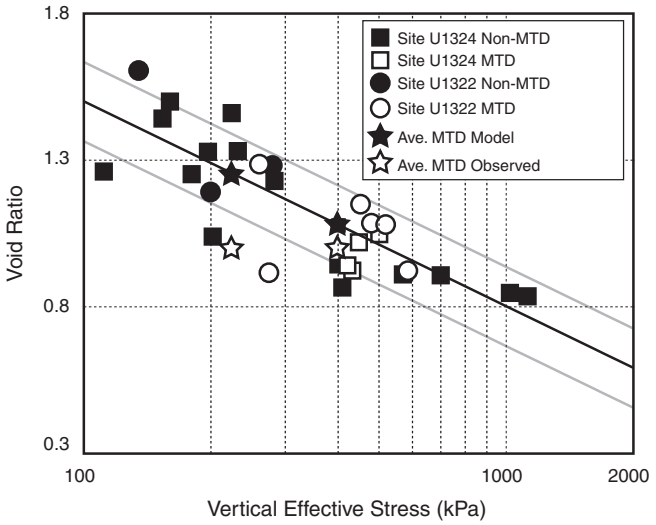

Fig. 7. Void ratio-vertical effective stress constraints for mud samples from Sites U1322 (circles) and U1324 (squares). Solid squares and circles are non-MTD samples and open squares and circles are data MTD samples. Solid line is best-fit model to the non-MTD data from Sites U1322 and U1324. Grey lines are the uncertainty in the best-fit model of the non-MTD data. The majority of the MTD data fit the same consolidation trend (i.e., within the model uncertainty) as the non-MTD sediments. Solid stars are the average void ratio modeled (Eq. (4)) for the interpreted, average vertical effectives stress for the MTD at Site U1324 (110–160 mbsf) and the MTD at Site U1322 (85–125 mbsf). Open stars are the logging-derived average porosity for the same MTD units for the interpreted, average vertical effectives stress.

Uncertainty in the void ratio–effective stress model (Fig. 7) suggests that the lower void ratio observed in the MTD interval at Site U1324 may not be statistically significant. The lower void ratio observed in the MTD interval at Site U1322, however, is a measurable and significant difference (Fig. 7). The source of model error and uncertainty could be the result of different processes. One potential source of error is sample disturbance caused by the drilling and coring operations. Sample disturbance can result in errors on the interpreted preconsolidation stress for a sample (e.g., Santagata and Germaine, 2002). Errors in the preconsolidation stress estimation due to sample disturbance are uncontrollable and yield uncertainty in e_o and c_c.

A second source of potential error is variation in the compression behavior based on changes in grain size or mineralogy. The consolidation experiment data used to constrain Eq. (4) focused on samples with similar grain-size distributions (>50% clay-sized particles) and similar gamma ray values (Figs. 3, 5). I interpret this reflects similar mineralogy of the sample intervals. Bulk mineralogical analyses from X-ray diffraction analyses of sediments from Site U1324 confirm a relatively homogeneous composition in the upper 360 mbsf consisting of 25% quartz and 35–39% phyllosilicates (John and Adatte, 2009). Based on similar grain-size distribution and composition of the MTD intervals and their bounding muds (i.e., 0–360 mbsf at Site U1324 and 0–240 mbsf at Site U1322), the sediments should have similar compression behavior (e.g., Skempton, 1970; Burland, 1990).

Through consolidation experiments on samples from Site U1324, Long et al. (2011) documented a single compression behavior for the muds from the Ursa region. This compression relationship, which was

defined from non-MTD muds at Site U1324, was used to estimate in situ pore pressures from void ratio data. These pressures matched those measured in situ in non-MTD intervals at Sites U1322 and U1324 (Long et al., 2011). Forward basin models of the Ursa region using this compression model also predict pressures that match the in situ observations (Stigall and Dugan, 2010). The ability to successfully invert measured void ratio for in situ pressure and to forward model the pressure genesis during sedimentation with one compression behavior supports the use of a single compression model to capture the primary deformation behavior in these sediments.

From the constraints on mineralogy and sedimentology and the ability to predict in situ conditions from uniform sedimentary properties, I interpret that one compression relation captures the majority of the deformation behavior of the mud-rich MTDs and non-MTD muds at Sites U1322 and U1324. The sample disturbance, however, is a source of error that must be considered when interpreting the void ratio-effective stress data of these sediments. The interpreted decrease of 2 porosity units, on average, in the MTD at Site U1324 cannot be confidently related to porosity loss from shear as it is within the model uncertainty (Fig. 7). The average decrease of 6 porosity units in the MTD at Site U1322 exceeds the model uncertainty and thus these sediments do show excess porosity loss relative to the non-MTD sediments (Figs. 5, 7). I infer this as shear-induced porosity loss due to the longer run-out of the MTDs at Site U1322. The MTD sediments at U1324 may have been losing porosity during shear, but not enough deformation was accumulated to differentiate it from the normal compaction trend interpreted from the preconsolidation stress data.

7. Discussion

Seismic and log data are integrated to define the physical properties of MTDs. I observe a lack of coherent internal structure in MTDs at local and regional scales. This is recorded as low amplitude, non-continuous reflections in the seismic data. These MTDs consistently have strong reflections at their bases. These strong reflections are controlled by sharp variations in physical properties. Log-measured density at all three sites in the Ursa region document that MTDs are denser than the under- and overlying non-MTD sediment, and that individual MTDs generally get denser with depth. This creates a large density contrast at the base of MTDs, which helps to create a large impedance contrast. This impedance contrast creates a high amplitude reflection. This suggests that from seismic data alone, it is possible to interpret sharp density contrasts from the amplitude character at the transition from MTDs to non-MTD mud. This could help when trying to develop drilling and sampling strategies.

The densification within MTDs is caused by shear strain and consolidation during movement and emplacement of MTDs. Densification during shear is common for highly sensitive clays, and shipboard strength experiments document intermediate to high sensitivity (ratio of peak shear strength to residual shear strength often exceeding 5 with maximum values exceeding 15) of the sediment at Sites U1322 and U1324 (Flemings et al., 2006). Triaxial experiments on sediments from Sites U1322 and U1324 also show contractional behavior during shear, which would lead to densification. Triaxial experiments by Meissl et al. (2010) document contraction during shear for relatively small axial strains (~2%) followed by dilation at higher axial strains; this dilational response, however, was likely controlled by the experiments being conducted on samples in an overconsolidated state. Triaxial compression tests on normally consolidated samples (overconsolidation ratio = 1) showed contraction during shear for axial strains up to 20% (Dugan and Germaine, 2009). Together the intermediate to high sensitivity of the mud-dominated sediments and the contractional behavior of the materials during triaxial experiments support fabric collapse and densification during shearing that created the MTDs at Ursa. This contractional behavior also suggests that that initial failure occurred when the samples were at an overconsolidation ratio near 1, which would have been the case if failure occurred at or near the seafloor (i.e., top of the MTD coincident with the seafloor). This leads to a conceptual model for failure where the sediments were initially deposited as part of the levee system and failure occurred from the seafloor to a discrete, shallow depth that defined the base of the slide. The failure stabilized and was preserved as an MTD, which was then buried by other levee deposits. This model assumes all levee deposits, whether part of a MTD or not, had a similar initial condition. While a spatially variable depositional or stress history for the levee deposits cannot be excluded based on the existing seismic, petrophysical, and geotechnical data, the regional stratigraphy, sedimentology, and modern depositional patterns support a regionally consistent depositional pattern for levee deposits in the Mississippi Canyon channel–levee systems. Failure of these deposits near the seafloor is consistent with sedimentation and stability models of the Ursa region that predicted failures were initiated in shallow, near-seafloor sediments and the timing of failure correlated with pulses of very high sedimentation (Stigall and Dugan, 2010).

The bases of the MTDs across the Ursa region are characterized by large density contrasts with the underlying mud. Localized deformation at the base of submarine slides has been observed in flume experiments of subaqueous gravity flows (DeBlasio et al., 2004). The sediments immediately below the tops of MTDs and the sediments immediately overlying the MTDs at Sites U1324 and U1322 have similar density (Figs. 3, 5). These similar densities do not produce a large impedance contrast, and thus do not produce a large seismic response at the top boundary of the MTDs. Even where the density, and thus impedance, contrasts are not strong, analysis of the regional seismic data, identification of the base of the MTDs, and then defining the seismic character of the MTDs can help to identify the tops of MTDs. For example, MTD2 in the Ursa (Fig. 2b) region has a strong, regionally continuous reflection that defines its base (Fig. 2a). The internal character of the MTD is low amplitude, discontinuous seismic reflections that overly the high amplitude base. The transition from the internal, poorly defined reflections to continuous amplitude reflections marks the top of MTD2 in the Ursa region (Fig. 2). Analysis of MTDs in the Nankai forearc in 3D seismic data reveals similar seismic architecture: low amplitude internal reflections with short lateral connectivity and top and bottom MTD-bounding reflections that are well defined and continuous (Strasser et al., 2011). In some cases (e.g., Site U1323) the top of the MTD has sharp physical property contrasts (Fig. 4) resulting in well defined, seismically imageable tops, which makes the identification simple in log and seismic data. Overall, these analyses suggest that the physical properties of MTDs produce a distinct seismic character that facilitates their identification in many settings; in some instances the identification correlates with abrupt, step changes in physical properties (e.g., base of MTD2 at Sites U1322, U1323, and U1324), but in some instances the tops are less well defined in the physical property data (top of MTD2 at Sites U1322 and U1324).

Resistivity data in the Ursa region provide a useful tool to identify slumps, deformation, and consolidation (Figs. 3–5, 7). The increase in resistivity in MTDs at Ursa is the result of densification and porosity loss within the MTDs. Because of the power-law relation between resistivity and porosity, the response is more pronounced in the resistivity logs. The increased resistivity in the MTDs is controlled by porosity loss due to increased vertical effective stress from burial and shear deformation from MTD mobilization. Anisotropy of magnetic susceptibility (AMS) analyses of sediments from Site U1322 and U1324 show that grains in non-MTD mud have no preferred orientation, whereas mud within the MTDs record grain re-arrangement during shearing as a preferred alignment of particles (Yamamoto et al., 2005). The AMS work also showed a higher degree of alignment in MTD sediments at Site U1322 than at Site U1324 (Yamamoto et al., 2005). Sawyer et al. (2009) interpreted a larger incremental volumetric strain at Site U1322 MTDs in comparison to Site U1324 and associated this larger strain with longer run-out of material at Site U1322. This larger strain is consistent with

increased grain alignment from shear. The larger strain also corresponds with the void ratio model I developed for Ursa with Site U1322 had an estimated porosity decrease of 6 porosity units, whereas Site U1324 potentially had a decrease of 2 porosity units. The high resistivity contrasts I observe between MTDs and bounding sediments are consistent with these data showing that more deformation has occurred in MTDs at Site U1322 compared to that at Site U1324.

My resistivity model and the LWD data, however, do not support anisotropy development at the bed scale (0.1–1 m). The simple resistivity-porosity relationship constrained in shallow, non-MTD mud at Site U1324 successfully predicts the observed resistivity in MTD and non-MTD mud at Sites U1322, U1323, and U1324 (Figs. 3–5). The robustness of this resistivity-porosity relationship indicates that at the bed-scale, anisotropic fabrics are not being generated. The same coefficients a, m in the Archie relationship suggest that at the log- or bed-scale, porosity and resistivity follow a normal consolidation trend indicative of uniaxial burial or that not enough shear strain has been accumulated to create a different fabric or sediment structure in the MTDs at Ursa. If significant fabric development were present, it is expected that the resistivity-porosity behavior would change as pore shapes and tortuosity change, therefore a and m would change. Comparison of multiple resistivity logs, which sample different length scales and azimuths, from IODP Sites U1322, U1323, and U1324 support the interpretation that different fabrics are not developed at the log scale for sediments in the Ursa region.

Analysis of the interpreted in situ effective vertical stresses from MTDs at Site U1322 and U1324 indicate they follow a similar uniaxial consolidation trend (Fig. 7). The void ratio-vertical effective stress (e-σ_v') data for all but one of the MTD samples are within the uncertainty of the e-σ_v' model derived for the non-MTD samples which indicates that there is no statistical difference in the compression behavior, as defined by the void ratio and preconsolidation stress data, of the non-MTD and MTD sediments. The similar compression behavior for Ursa sediment suggests that grain re-arrangement and porosity loss for mud subject to uniaxial burial and for MTDs subject to burial, shear, and burial follow the same porosity-stress pathway. If separate fabrics or soil structures existed between the MTDs and the non-MTD mud, they would have different compression behavior defined by different e_o and c_c. (e.g., Leroueil et al., 1985; Burland, 1990). The consistent deformation behavior allows some extrapolation of the in situ physical properties of the MTD sediments from the properties of the normally consolidated mud. At the simplest level, it provides a means to estimate the amount of shear-induced consolidation within the MTDs and also regional comparison of shear. From the data at Sites U1322 and U1324, I document increased shear deformation at Site U1322 in comparison to Site U1324. This indicates longer MTD run-out at Site U1322.

This additional porosity loss in the MTDs has implications for fluid flow and overpressure in the Ursa region. Decreased porosity from shear consolidation creates lower permeability of MTDs at shallow depths. Schneider et al. (2008) define the vertical permeability of mudstones at Ursa as a function of porosity, $\log(k) = 9.0\phi - 22.2$. From this relation and the porosity loss due to shear consolidation, I estimate the MTD at Site U1324 has a 33% permeability decrease with respect to normally consolidated, non-MTD mud. The larger porosity loss (6 porosity units) at Site U1322, equates to a 71% decrease in permeability when compared to normally consolidated sediments. The decrease in permeability enhances the seal capacity of MTDs, which helps to preserve the high overpressure even as sedimentation rates have decreased.

Pore fluid expulsion during shear may also induce overpressure. One-dimensional sedimentation-consolidation models cannot explain the overpressures in the Ursa region without additional fluid sources. Lateral transfer of fluids through the Blue Unit from the west to the east provides a fluid sink at Site U1324 and a fluid source at Site 1322, and has been invoked as a primary contributor to the overpressure field (Dugan and Germaine, 2008; Flemings et al., 2008; Stigall and Dugan, 2010). Shear consolidation and porosity loss within MTDs at Ursa provide another fluid pressure source. This additional source could contribute to the shallow onset of overpressure especially within MTDs. The pressure source could also contribute to the retrogressive behavior of failures in the Ursa basin (e.g., Sawyer et al., 2009).

Preservation of enhanced densification and porosity loss within MTDs relative to the bounding mud is required to create the seismic response and to consider MTDs as potential sealing units at depth after burial. Traditional soil mechanics models indicate that during burial, a soil will follow a normal compression curve (e.g., e–σ_v' curve) that is characteristic of that soil (e.g., Burland, 1990; Wood, 1990). A subsequent shearing event, such as that to create the MTDs at Ursa, will shift the soil to a different compression curve defined by the critical state of the soil. A return to uniaxial burial after failure then returns the soil to the normal compression curve, thus erasing any shear-induced structure or perturbation to the sample (e.g., Wood, 1990). This model implies that after sufficient burial, no density or porosity contrast would exist between the MTDs or the bounding mud, thus there would not be an impedance contrast and the MTDs would not have well defined seismic boundaries. The observations at Ursa, however, document that some of the densification during shear is preserved after burial as imaged in the resistivity data, the density data, and the seismic response at the top and bottom of the MTDs. At Sites U1322, U1323, and U1324, the depth of MTD2 is 2 to 5 times greater than its original thickness (Fig. 2). Thus the densification is preserved at effective vertical stresses 2 to 5 times greater than then effective vertical stresses at failure. Analysis of the thinner, deeper MTDs that comprise MTD1 at Site U1322 exemplify this point; these thin MTDs have been buried to depths 15 times greater than their original thickness, but their physical properties still differ from the bounding mud (Fig. 5).

The preserved difference in physical properties and resulting seismic response is not limited to the Ursa region. Seismic structure of the Storegga Slide offshore Norway shows distinct bounding reflections that indicate portions of the slide have been buried 2.5 to 5 times its original thickness (Solheim et al., 2005). Along the Amazon Fan, MTDs that have been buried to twice their original thickness retain different resistivity and seismic character from the bounding sediments (Piper et al., 1997). Mass transport deposits on the slope of the Nankai accretionary complex also have well defined seismic tops and bottoms; the depth-to-thickness ratios of some slides of the Nankai forearc range range from 3 to 5 (Strasser et al., 2011). The prevalence of high amplitude contrasts at the tops and/or bases of MTDs and the depth-to-thickness ratios at numerous locations suggests that the physical changes imparted on the soil during shear may not be erased during burial, or that the changes are not erased until burial proceeds to significant depth. While the observations of densification and seismic response are consistent for multiple MTDs, the mechanism that preserves of these physical behaviors requires additional analysis on the post-shear deformation.

8. Conclusions

I integrated seismic data, logging-while-drilling (LWD) data, and consolidation data from core samples to document that MTDs have increased resistivity and bulk density in comparison to non-deformed sediments in the Ursa region. The increase in resistivity is caused by densification of the MTDs. Densification of Ursa sediments is confirmed by their high sensitivity and triaxial experiments on normally consolidated samples. The bulk density within MTDs generally increases with increasing depth through MTDs creating an abrupt density contrast between the base of MTDs and the underlying mud. The density contrast at the base of the MTDs creates a strong, easily identifiable reflection in multi-channel seismic data. The density contrast that controls the seismic response allows seismic data to be used to infer density contrasts between hemipelagic drape and MTDs in many geologic settings.

Analysis of consolidation state (preconsolidation stress and void ratio) shows that MTDs follow the same trend as uniaxially buried mud in the Ursa region. The consistent resistivity-porosity and consolidation relations for MTD mud and hemipelagic, uniaxially consolidated mud in the Ursa region are interpreted to reflect an absence of bed-scale fabric development altering deformation behavior of MTDs, even though there is enhanced shear deformation of up to 6 porosity units in the MTDs. This research documents that resistivity and bulk density data can be used to characterize the amount of shear deformation in submarine MTDs, to compare the relative amounts of deformation within MTDs, and can be used to explain the seismic response of MTDs in shallow sediments. Increased density of MTDs may also result in fluid sources and lower permeability that may help generate overpressure during MTD emplacement and may help preserve overpressure over long time periods and burial.

Acknowledgements

Shell International Exploration and Production Incorporated and the Ursa partners provided access to seismic data that were used in this study. These data motivated my investigation of MTDs and were critical to planning the IODP operations. This work benefited from the dedication and efforts of the participants and technical staff of IODP Expedition 308. This research used data provided by the Integrated Ocean Drilling Program (IODP). Funding for this research was provided by the Consortium for Ocean Leadership. Paradigm's Geolog® software was used to process and display log data. Three anonymous reviewers and David Piper are thanked for comments that have improved this paper.

References

Archie, G.E., 1942. The electrical resistivity log as an aid in determining some reservoir characteristics. Transactions American Institute of Mining, Metallurgical, and Petroleum Engineers 146, 54–62.

Becker, D.E., Crooks, J.H.A., Been, K., Jefferies, M.G., 1987. Work as a criterion for determining in situ and yield stresses in clays. Canadian Geotechnical Journal 24, 549–564.

Bull, S., Cartwright, J., Huuse, M., 2009. A subsurface evacuation model for submarine slope failure. Basin Research 21, 433–443. http://dx.doi.org/10.1111/j.1365-2117.2008.00390.x.

Burland, J.B., 1990. On the compressibility and shear strength of natural clays. Geotechnique 40 (3), 329–378.

DeBlasio, F.V., Ilstad, T., Elverhoi, A., Issler, D., Harbitz, C.B., 2004. High mobility of subaqueous debris flows and the lubricating-layer model. Proceedings of the Offshore Technology Conference, Houston, TX. Paper OTC 16747.

Dugan, B., Germaine, J.T., 2008. Near-seafloor overpressure in the deepwater Mississippi Canyon, northern Gulf of Mexico. Geophysical Research Letters 35, L02304. http://dx.doi.org/10.1029/2007GL032275.

Dugan, B., Germaine, J.T., 2009. Data report: strength characteristics of sediments from IODP Expedition 308, Sites U1322 and U1324. Proceedings of the Integrated Ocean Drilling Program 308. http://dx.doi.org/10.2204/iodp.proc.308.210.2009.

Eaton, L.F., 1999. Drilling through deepwater shallow water flow zones at Ursa. Proceedings of the SPE/IADC Middle East Drilling Conference, pp. 153–164.

Flemings, P.B., Behrmann, J.H., John, C.M., The Expedition 308 Scientists, 2006. Proceedings of the Integrated Ocean Drilling Program 308. Integrated Ocean Drilling Program Management International, Inc., College Station TX. http://dx.doi.org/10.2204/iodp.proc.308.2006.

Flemings, P.B., Long, H., Dugan, B., Germaine, J., John, C.M., Behrmann, J.H., Sawyer, D., Expedition 308 Scientists, 2008. Pore pressure penetrometers document high overpressure near the seafloor where multiple submarine landslides have occurred on the continental slope, offshore Louisiana, Gulf of Mexico. Earth and Planetary Science Letters 274 (1–2), 269–283. http://dx.doi.org/10.1016/j.epsl.2008.06.027.

Hampton, M.A., Lee, H.J., Locat, J., 1996. Submarine landslides. Reviews of Geophysics 34 (1), 33–59.

John, C., Adatte, T., 2009. Data report: X-ray analyses of bulk sediment in IODP Holes U1320A and U1324B, northern Gulf of Mexico. Proceedings of the Integrated Ocean Drilling Program 308. http://dx.doi.org/10.2204/iodp.proc.308.214.2009.

Kvalstad, T.J., Andersen, L., Forsberg, C.F., Berg, K., Bryn, P., Wangen, M., 2005. The Storegga slide: evaluation of triggering sources and slide mechanics. Marine and Petroleum Geology 22, 245–246. http://dx.doi.org/10.1016/j.marpetgeo.2004.10.019.

Lambe, T.W., Whitman, R.V., 1969. Soil Mechanics. John Wiley & Sons, New York. 553 pp.

Leroueil, S., Tavenas, F., Locat, J., 1985. Discussion to "Correlations between index tests and the properties of remolded clays" by Carrier and Beckman. Geotechnique 35 (2), 223–226.

Locat, J., Lee, H., ten Brink, U.S., Twichell, D., Geist, E., Sansoucy, M., 2009. Geomorphology, stability and mobility of the Currituck slide. Marine Geology 264 (1–2), 28–40. http://dx.doi.org/10.1016/j.margeo.2008.12.005.

Long, H., Flemings, P.B., Dugan, B., Germaine, J.T., Ferrell, D., 2008a. Data report: penetrometer measurements of in situ temperature and pressure, IODP Expedition 308. Proceedings of the Integrated Ocean Drilling Program 308. http://dx.doi.org/10.2204/iodp.proc.308.203.2008.

Long, H., Flemings, P.B., Germaine, J.T., Saffer, D.M., Dugan, B., 2008b. Data report: consolidation characteristics of sediments from IODP Expedition 308, Ursa Basin, Gulf of Mexico. Proceedings of the Integrated Ocean Drilling Program 308. http://dx.doi.org/10.2204/iodp.proc.308.204.2008.

Long, H., Flemings, P.B., Germaine, J.T., Saffer, D.M., 2011. Consolidation and overpressure near the seafloor in the Ursa Basin, Deepwater Gulf of Mexico. Earth and Planetary Science Letters 305, 11–20. http://dx.doi.org/10.1016/j.epsl.2011.02.007.

McAdoo, B.G., Pratson, L.F., Orange, D.L., 2000. Submarine landslide geomorphology, US continental slope. Marine Geology 169, 103–136.

Meissl, S., Behrmann, J., Behrmann, J.H., 2010. Data report: preliminary assessment of Pleistocene sediment strength in the Ursa Basin (Gulf of Mexico continental slope) from triaxial and ring shear test data. Proceedings of the Integrated Ocean Drilling Program 308. http://dx.doi.org/10.2204/iodp.proc.308.211.2010.

Ostermeier, R.M., Pelletier, J.H., Winker, C.D., Nicholson, J.W., Rambow, F.H., Cowan, K.M., 2000. Dealing with shallow-water flow in the deepwater Gulf of Mexico. Proceedings of the Offshore Technology Conference. Paper OTC 11972.

Ostermeier, R.M., Pelletier, J.H., Winker, C.D., Nicholson, J.W., 2001. Trends in shallow sediment pore pressures. Proceedings of the Society of Petroleum Engineers/International Association of Drilling Contractors Drilling Conference, Paper SPE/IADC 67772, 1–11.

Pelletier, J.H., Ostermeier, R.M., Winker, C.D., Nicholson, J.W., Rambow, F.H., 1999. Shallow water flow sands in the deepwater Gulf of Mexico: some recent shell experience. International Forum on Shallow Water Flows Conference, League City, TX, 6–9 Oct.

Piper, D.J.W., Pirmez, C., Manley, P.L., Long, D., Flood, R.D., Normark, W.R., Showers, W., 1997. Mass-transport deposits of the Amazon fan. Proceedings of the Ocean Drilling Program, Scientific Results 155, 109–146.

Posamentier, H., 2004. Stratigraphy and geomorphology of deep-water mass transport complexes based on 3D seismic data. Offshore Technology Conference. Paper OTC16740.

Santagata, M.C., Germaine, J.T., 2002. Sampling disturbance effects in normally consolidated clays. Journal of Geotechnical and Geoenvironmental Engineering 128 (12), 997–1006. http://dx.doi.org/10.1061/(ASCE)1090-0241(2002)128:12(997).

Sawyer, D.E., Flemings, P.B., Shipp, R.C., Winker, C.D., 2007. Seismic geomorphology, lithology, and evolution of the late Pleistocene Mars-Ursa turbidite region, Mississippi Canyon area, northern Gulf of Mexico. AAPG Bulletin 91 (2), 215–234. http://dx.doi.org/10.1306/08290605190.

Sawyer, D.E., Jacoby, R., Flemings, P.B., Germaine, J.T., 2008. Data report: particle size analysis of sediments in the Ursa basin, IODP Expedition 308 Sites U1324 and U1322, northern Gulf of Mexico. Proceedings of the Integrated Ocean Drilling Program 308. http://dx.doi.org/10.2204/iodp.proc.308.205.2008.

Sawyer, D.E., Flemings, P.B., Dugan, B., Germaine, J.T., 2009. Retrogressive failures recorded in mass transport deposits in the Ursa Basin, Northern Gulf of Mexico. Journal of Geophysical Research 114, B10102. http://dx.doi.org/10.1029/2008JB006159.

Schneider, J., Flemings, P.B., Dugan, B., Long, H., Germaine, J.T., Saffer, D.M., 2008. Porosity vs. permeability behavior of shallow mudstones in the Ursa Basin, deepwater Gulf of Mexico. EOS Transactions of the American Geophysical Union 89 (53) (Fall Meeting Supplement. Abstract OS11A-1105).

Skempton, A.W., 1970. The consolidation of clays by gravitational compaction. Quarterly Journal of the Geological Society 125, 373–411. http://dx.doi.org/10.1144/gsjgs.125.1.0373.

Solheim, A., Berg, K., Forsberg, C.F., Bryn, P., 2005. The Storegga Slide complex: repetitive large scale sliding with similar cause and development. Marine and Petroleum Geology 22, 97–107.

Stigall, J., Dugan, B., 2010. Overpressure and earthquake initiated slope failure in the Ursa region, northern Gulf of Mexico. Journal of Geophysical Research 115, B04101. http://dx.doi.org/10.1029/2009JB006848.

Strasser, M., Moore, G.F., Kimura, G., Kopf, A.J., Underwood, M.B., Guo, J., Screaton, E.J., 2011. Slumping and mass transport deposition in the Nankai fore arc: evidence from IODP drilling and 3-D reflection seismic data. Geochemistry Geophysics Geosystems 12 (5), Q0AD13. http://dx.doi.org/10.1029/2010GC003431.

Winker, C.D., Booth, J.R., 2000. Sedimentary dynamics of the salt-dominated continental slope, Gulf of Mexico: integration of observations from the seafloor, near-surface, and deep subsurface. Proceedings of Gulf Coast Section of the Society for Sedimentary Geology (GCSSEPM) 20th Annual Research Conference, pp. 1059–1086.

Wood, D.M., 1990. Soil Behavior and Critical State Soil Mechanics. Cambridge University Press, Cambridge. 462 pp.

Yamamoto, Y., Sawyer, D.E., Behrmann, J.H., Flemings, P.B., John, C.M., IODP Expedition 308 Shipboard Scientific Party, 2005. Fabric contribution to sediment physical properties in Gulf of Mexico: preliminary results of IODP Expedition 308. EOS Transactions of the American Geophysical Union 86 (52) (Fall Meeting Supplement. Abstract OS21A-1514).